EurJIC
European Journal of Inorganic Chemistry

Research Article
doi.org/10.1002/ejic.202400222

Chemistry Europe
European Chemical Societies Publishing

www.eurjic.org

Hot Paper

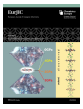

Pressure-Induced Encapsulation of Cs^+ Cations within an 18-Crown-6 Cavity: Insights from X-ray Diffraction, Raman Spectroscopy, and DFT Calculations

Eduard B. Rusanov,*[a, b] Michael D. Wörle,[a] Maksym V. Kovalenko,[a, c] Kostiantyn V. Domasevitch,[d] and Julia A. Rusanova[d]

This study utilizes single-crystal X-ray diffraction in a diamond anvil cell (DAC) to explore the structural response of [Cs(18-Crown-6)][SbCl6] under high pressure (HP). Notably, the pressure drives large Cs atoms closer to the center of the crown ether cavity, ultimately requiring pressures of 3 GPa for its complete encapsulation. Remarkably, the absence of short contacts in the crystal classifies the material as a "loose crystal" offering a unique model for understanding compression mechanisms. The crystal exhibits highly anisotropic compression behavior with an impressive volume reduction and non-linear pressure – unit-cell parameters relationships facilitated by the absence of short CH···Cl contacts up to 0.9 GPa. Beyond this pressure, steric repulsion due to shortening H···Cl and H···H interactions hinders further effective compression, so pressure dependence on unit cell parameters and volume becomes more linear. The behavior of [Cs(18-Crown-6)][SbCl6] at different conditions was studied using Raman spectroscopy and supplemented by DFT calculations.

Introduction

The exceptional properties of macrocyclic compounds make them valuable tools for the solid-state design of diverse materials.[1] The unique structure of the 18-crown-6, allows it to form highly stable host-guest complexes, especially with different inorganic and organic cations, such as alkali metals and primary amine due to the formation of multiple metal-oxygen and hydrogen bonds with oxygen atoms. This makes 18-crown-6 containing compounds a versatile and important class of materials with a wide range of potential applications, including catalysis,[2] ions separation,[3] sensors,[4] drug delivery,[5] and materials science.[6,7] Of particular note is the growing interest in halide perovskites for optoelectronic applications.[8,9]

The unique ability to finely control the coordination geometries of anionic metal halide octahedra and $M(18\text{-crown-6})^+$ counterparts through variation of the ionic radii of encapsulated M^+ cations drives this phenomenon.[10,11] Therefore, understanding the inherent solid-state structural trends of $[M(18\text{-crown-6})]^+$ complexes is crucial for designing materials with desired optoelectronic properties and the positioning of alkali metal cations within the macrocyclic cavity exhibits intriguing variations. Unlike $[K(18\text{-crown-6})]^+$ species, where the small K^+ cations usually perfectly fit within the macrocyclic cavity,[1] larger Rb^+ cations exhibit more diverse positioning. The Rb^+ cations mostly remain at large distances 0.8–1.2 Å above the plane. Nevertheless, crystal field forces can position the Rb^+ cation very close to the cavity less than 0.25 Å[12] or even within it. This enables perfect fitting of the cavity with Rb^+ cations using an alternating centrosymmetric arrangement of singly charged cations with oximates[13] or $AuCl_4^-$.[14] The centrosymmetric arrangement of cations and anions, proven successful for Rb^+ and Tl^+ cations within crown ether cavities, holds promise for accommodating the larger Cs^+ cation. Nevertheless, larger Cs^+ cations consistently locate themselves significantly above the crown ether. According to a Cambridge Structural Database (CSD) search,[15] typical deviations of Cs^+ in $[Cs(18\text{-crown-6})]^+$ cations are reported(see Figure 1) to be 1.2–1.8 Å above the center of the crown ether Cavity. Deviations exceeding this range indicate the formation of sandwich[16,17] or triple-decker sandwich[18,19] structures with Cs^+ cations located up to 2.5 Å above the crown ether plane. Only two known examples exist where the Cs^+ cation resides within about 1 Å above the plane of the crown ether and involve specific scenarios: in $[Cs(18\text{-crown-6})]^+$ sandwiched between two large planar moieties[20] and in the structure where cations alternate with bridged $SbCl_6^-$ anions.[21] The latter scenario exhibits the smallest observed out-of-plane deviation of the Cs^+ cation (0.934 Å). Each of these examples falls into a category of forced geometries, and therefore the placement of Cs^+ ions close to

[a] Dr. E. B. Rusanov, Dr. M. D. Wörle, Prof. M. V. Kovalenko
Department of Chemistry and Applied Biosciences,
ETH Zürich
Vladimir Prelog Weg 1, Zürich, CH-8093, Switzerland
E-mail: erusanov@ethz.ch

[b] Dr. E. B. Rusanov
Institute of Organic Chemistry at National Academy of Sciences of Ukraine,
Academik Kukhar Str. 5, Kyiv, 02094, Ukraine

[c] Prof. M. V. Kovalenko
Empa – Swiss Federal Laboratories for Materials Science and Technology
Überlandstrasse 129, CH-8600 Dübendorf, Switzerland

[d] Prof. K. V. Domasevitch, Dr. J. A. Rusanova
Department of Chemistry
Taras Shevchenko National University of Kyiv,
Volodymyrska Str. 64/13, 01601 Kyiv, Ukraine

Research Article
doi.org/10.1002/ejic.202400222

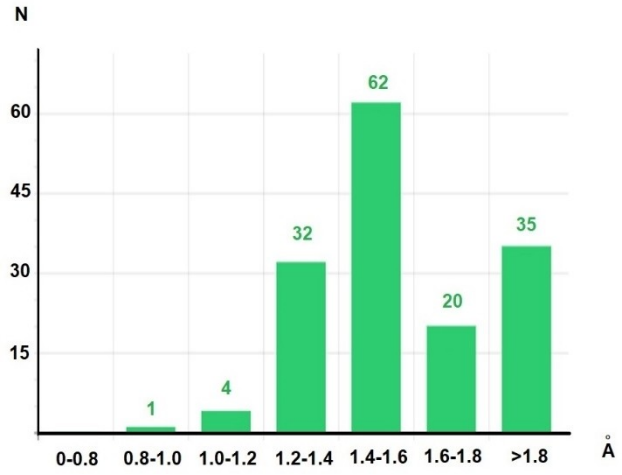

Figure 1. Histogram of frequency of observations the Cs^+ cation above the mean-square plane of six oxygen atoms of 18-crown-6 according to data from a CSD search.

the 18-crown-6 cavity inevitably relied on the "pressure of the crystal environment", demonstrating the effectiveness of the centrosymmetric arrangement. Despite this progress, achieving an ideal location of Cs^+ within the crown ether cavity remains impossible using traditional chemical structure design methods. However, a similar structural output for crystal structure tuning may be achieved by applying the forces of the external stimuli such as high pressure in GPa range, which themselves are simpler to understand and measure. Pressure has the most profound effect on weak non-covalent interactions within the crystal lattice. These include CH···X,[22,23] X···X[24] (where X is a halogen), and H···H[25,26] interactions. These pressure-induced structural changes often exceed those achieved through temperature manipulation alone.[27] Due to the inherent anisotropy of crystals, pressure rarely acts uniformly. This leads to anisotropic deformation, where different crystallographic directions experience varying degrees of compression. The study of non-covalent interactions provides extremely valuable information[28] about materials, as anisotropy can also promote phase transitions by minimizing interactions between closely packed molecules.[29]

In the present work, we explore such an attractive possibility with a closer look at the previously reported [Cs(18-Crown-6)][$SbCl_6$] complex,[21] which was selected for a range of particular features. Considering the significantly larger deviation of the cesium atom, we can expect that the corresponding cesium complex can be structurally adjusted over a wider range of geometric parameters when changing pressure. Also, a clear structural response of the $[Cs(18\text{-crown-6})]^+$ system to such extreme conditions, with the simple parameter of Cs^+-18-crown-6 center separation as a function of the applied pressure is expected in an HP diffraction experiment. The [Cs(18-Crown-6)][$SbCl_6$] complex has two remarkable structural features that make it ideal for studying the effects of pressure on cation positioning within crown ether cavities: *i*) it exhibits the smallest observed deviation of a disordered Cs^+ cation from the crown ether plane among all known compounds; *ii*) the compound features one-dimensional chains alternating high-symmetry, centrosymmetric $[Cs(18\text{-crown-6})]^+$ cations and $[SbCl_6]^-$ anions situated on 3-fold axis. The separation between disordered Cs^+ positions (twice the distance between the crown ether center and the metal) serves as a sensitive indicator for monitoring pressure-induced changes. Also, the high metric symmetry (trigonal R-3) and completely ordered macrocyclic ring enhance the capabilities of HP diffraction data acquisition using a diamond anvil cell (DAC). In addition, the good overall scattering ability of the crystal at room temperature further enhances its potential for diffraction studies.

Results and Discussion

Ambient-Pressure Structure

In the crystal structure of the named complex cationic $[Cs(18\text{-crown-6})]^+$ and anionic $SbCl_6^-$ species are situated on the 3-fold axis and centers of inversion, so the independent part consists of only a one-sixth complex moiety. According to the symmetry, the crown ether molecule adopts the D_{3d} conformation. The Cs cations are equally disordered over the center of inversion and occupy two equivalent positions, above and below the mean square plane of six oxygen atoms of the crown ether (see Figure 2).

A significant feature is cooling to 100 K, which leads not only improving for displacement ellipsoids but also to a shortening of the distance between two components of the disordered Cs^+ cations from 1.8977(16) Å to 1.7157(8) Å. This observation suggests that Cs^+ cations tend to approach the center of the 18-crown-6 cavity as the temperature decreases, so the crystal should be very sensitive to applying HP. The molecular packing for this structure is represented by infinite chains along the c-axis (see Figure 3), consisting of alternating $[Cs(18\text{-crown-6})]^+$ cations and $SbCl_6^-$ anions, linked by set of Cs–Cl bonds at 3.5891(13) Å.

In a crystal present a very weak C2–H2B···Cl1 and C1–H1B···Cl1^{i} (i = *1/3 + x–y, −1/3 + x, 2/3−z*) interactions directed along 0z directions with the following parameters H2B···Cl1 3.24 Å, C2–H2b···Cl1 150° and H1B···Cl1^{i} 3.42 Å, C2–H1b···Cl1^{i} 147° at ambient conditions (Figure 4). Additionally, the crystal exhibits weak C2–H2 A···Cl1^{ii} (ii = *1/3−y, −1/3 + x–y, −1/3 + z*) interactions, that extend in the *ab* plane between adjacent columns with a H2 A···Cl1^{ii} distance of 3.10 Å and a C2–H2 A···Cl1^{ii} angle of 130°. These intermolecular interactions are further characterized by the presence of the shortest H1B···H1A^{ii} contact 2.74 Å directed along the c-axis between adjacent columns. Based on the observed properties, the [Cs(18-Crown-6)][$SbCl_6$] crystal exhibits remarkable similarities to the previously studied Rb complex, suggesting it can also be categorized as a "loose crystal"[30] characterized by a contact parameter $\delta = 0.15$, defined as the shortest of all intermolecular contacts calculated as the difference of distance d_{ij} from atom *i* to atom *j* and their van der Waals (vdW) radii ($\delta = \min(d_{ij} - vdW_i - vdW_j)$). This reinforces the notion that the choice of alkali metal cation may not significantly impact the Figure 4.

Research Article
doi.org/10.1002/ejic.202400222

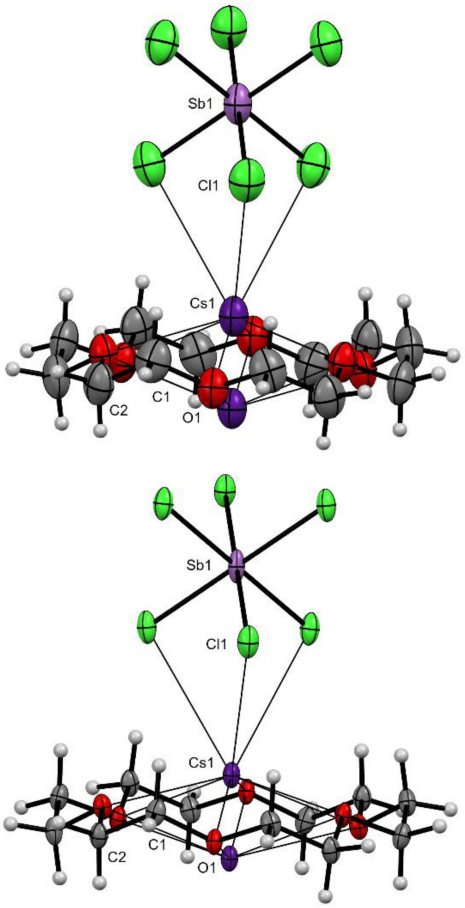

Figure 2. Structure of [Cs(18-Crown-6)][$SbCl_6$] at 293 K(top) and 100 K (down) with the displacement ellipsoids drawn at 50% probability level. Only independent non-hydrogen atoms are labeled. Two disordered positions for Cs cation are shown.

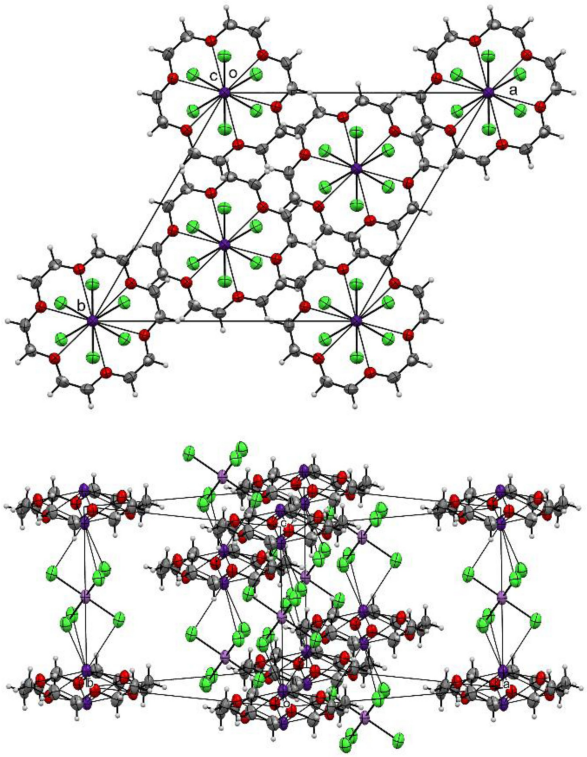

Figure 3. Molecular packing of the [Cs(18-Crown-6)][SbCl6] viewed along the *c* direction (top) and the orthogonal view of the unit cell (down).

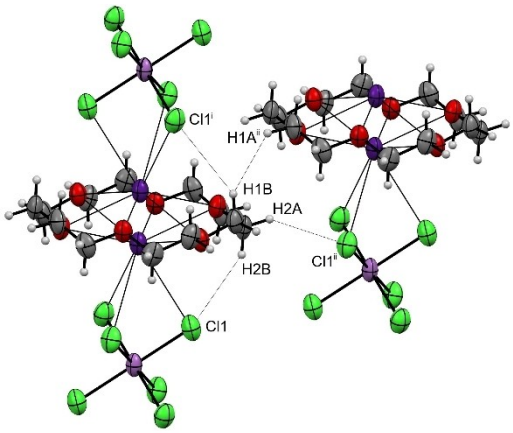

Figure 4. The shortest intra and intermolecular H···Cl and H···H contacts. Symmetry codes (i = *1/3 + x-y, −1/3 + x, 2/3−z;* ii = *1/3−y, −1/3 + x-y, −1/3 + z*).

The shortest intra and intermolecular H···Cl and H···H contacts. Symmetry codes (i = *1/3 + x–y, −1/3 + x, 2/3−z;* ii = *1/3−y, −1/3 + x–y, −1/3 + z*) overall nature of the crystal packing in this specific system. Although all these H···Cl and H···H interactions are longer than the sum of the vdW radii[31] for H/Cl and H/H pairs of atoms (2.95 and 2.40 Å respectively), they nevertheless play an important role in the subsequent discussion of contacts in a crystal under HP.

An intriguing comparison can be made between the unit cell parameters of [Cs(18-Crown-6)][$SbCl_6$] and recently studied [Rb(18-crown-6)][$SbCl_6$].[32] Notably, the lengths of the *a* and *b* unit-cell axes of the Cs compound are slightly shorter (0.0586(9) Å) than those of the Rb compound, while the axis *c* is significantly longer (0.4167(10) Å). The decrease in the *a* and *b* unit cell axes suggests more efficient packing of adjacent [Cs(18-crown-6)$^{+}SbCl_6^{-}$]$_n$ chains in the Cs complex compared to the Rb complex. Conversely, the increase in the axis *c* arises due to the larger Cs^+ cations deviating more significantly from the mean plane of the crown ether plane compared to the smaller Rb^+ cations. This observation is supported by the shorter H2 A···Cl1^{ii} contacts (3.10 Å) in *ab* plane and significantly longer H2Bb···Cl1 contacts (3.24 Å) along the *c* direction in the Cs complex compared to the Rb complex (3.11 Å and 3.08 Å, respectively). It is noteworthy that at room temperature, the Cs–Cl bond distances in [Cs(18-Crown-6)][$SbCl_6$] are unexpectedly shorter (3.5891(13) Å) than the Rb–Cl bond distances (3.7255(13) Å) in the corresponding complex. The former value is very close to the Cs–Cl distance of 3.574 Å in the CsCl crystal,[33] while the latter value is significantly longer than the Rb–Cl distance of 3.438 Å in the RbCl crystal.[34] This is surprising because the cationic radius of Cs^+ is larger than that of Rb^+ (1.67 and 1.52 Å, respectively), so it would be logical to expect

Research Article
doi.org/10.1002/ejic.202400222

Table 1. The unit cell parameters and refinement parameters in the crystal [Cs(18-Crown-6)][SbCl6] at various pressures.

Pressure (GPa)*	*a* (Å)	*c* (Å)	V (Å^3)	R_{int}	R1/wR2 (I > 2σ(I))	GOF	Δρ(e/Å^3)
0.0(100 K)	13.9881(6)	10.3114(6)	1747.29(18)	0.0239	0.0198/0.0447	1.050	0.75/−0.54
0.0	14.0626(9)	10.6441(10)	1822.9(3)	0.0252	0.0295/0.0724	1.048	1.74/−0.57
0.04	14.0603(8)	10.5698(13)	1809.6(3)	0.0356	0.0278/0.0685	1.029	0.44/−0.33
0.23	13.9990(8)	10.3595(13)	1758.2(3)	0.0315	0.0282/0.0606	1.037	0.44/−0.53
0.35	13.9658(8)	10.2456(14)	1730.6(3)	0.0356	0.0270/0.0643	1.038	0.50/−0.38
0.56	13.9212(7)	10.1100(13)	1696.8(3)	0.0382	0.0250/0.0609	1.025	0.40/−0.44
0.67	13.9028(8)	10.0318(15)	1679.3(3)	0.0289	0.0264/0.0636	1.009	0.49/−0.42
0.90	13.8578(7)	9.8916(13)	1645.1(3)	0.0280	0.0253/0.0625	1.032	0.43/−0.34
1.04	13.8384(7)	9.8210(12)	1628.8(3)	0.0302	0.0246/0.0597	1.021	0.37/−0.40
1.20	13.8043(6)	9.7524(12)	1609.4(2)	0.0279	0.0206/0.0459	1.048	0.34/−0.33
1.33	13.7883(6)	9.7046(10)	1597.8(2)	0.0277	0.0199/0.0474	1.019	0.39/−0.22
1.57	13.7549(6)	9.6213(11)	1576.4(2)	0.0285	0.0208/0.0509	1.033	0.29/−0.34
1.69	13.7423(7)	9.5988(13)	1569.9(3)	0.0312	0.0209/0.0423	1.023	0.38/−0.26
2.05	13.6928(11)	9.501(2)	1542.8(4)	0.0954	0.0695/0.1740	1.040	1.90/−1.26
2.05c					0.0697/0.1743	1.041	1.88/−1.30

c The Cesium atom was refined at the center of inversion. * Data collection for diffraction experiments performed at 293 K excluding the data collected at 100 K.

that the Cs–Cl bond distances would be longer than the Rb–Cl bonds in the corresponding compound. Apparently, the long Rb–Cl distances and relatively long shortest H···Cl and H···H contacts between molecules in a crystal were the primary factors contributing to the behavior of the loose Rb(18-crown-6)$SbCl_6$ crystal. Since the distance between crown ether and $SbCl_6^-$ anion in [Cs(18-Crown-6)][$SbCl_6$] is about 0.2 Å larger compared to the isostructural Rubidium complex, the shortest H···Cl contacts in the columns are significantly longer than the sum of their vdW radii. Thus, the large separation of the crown ether and the $SbCl_6^-$ anion suggests a potentially more efficient compression due to the lack of short H···Cl contacts in the direction of the crystallographic axis *c*. Such a larger distance can provide a more efficient displacement of the Cs^+ cation to the center of the crown ether cavity under pressure. However, shortening of the relevant contacts in the cesium complex is likely to occur only at significantly higher pressures, exceeding 1 GPa. This expectation is based on the observation that short contacts H···Cl were observed in the Rb complex only at pressures above 0.75 GPa. Therefore, to test this assumption and explore the possibility of encapsulating large Cs^+ cations within the crown ether cavity, a series of HP experiments were conducted on [Cs(18-Crown-6)][$SbCl_6$].

Response of the Unit-Cell Parameters to Applied Pressure

Information about the crystal data and main structure refinement details at various pressures are summarized in Table 1. Across the pressure range, the crystal structure response to hydrostatic pressure is anisotropic. The non-linear changes in the unit cell dimensions P-*a*/P-*c* and unit-cell volume P–V on pressure are shown in Figure 5. The *a*- and *b*-axes length exhibits a relatively small decrease within the pressure range of 0–2.05 GPa, contracting by only 0.3698(11) Å or 2.63 %, com-

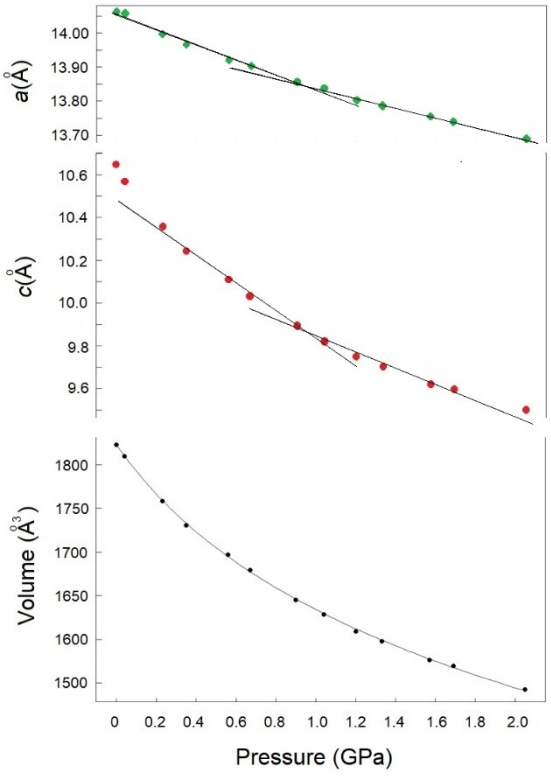

Figure 5. Unit-cell parameters *a*, *c* and *V* as a function of pressure in the [Cs(18-crown-6)][$SbCl_6$] crystal.

Research Article
doi.org/10.1002/ejic.202400222

pared to 0.4407(8) Å or 3.12% observed for the Rubidium complex at 1.89 GPa. Among the unit-cell parameters, the *c*-axis, as noted in Table 1, is the most compressible parameter, shortening by 1.143(2) Å or 10.74% upon increasing pressure to 2.05(3) GPa. This compression is significantly larger than the 0.7841(9) Å or 8.25% recently reported for the Rb complex at 1.89(3) GPa.[32]

It is noteworthy that at low pressures the *c*-axis exhibits significantly faster and more efficient compression than the *a*- and *b*-axes. For example, at 0.23(3) GPa, the *a*-axis only shortens by 0.0636(9) Å, while the *c*-axis exhibits a much larger contraction of 0.2846(14) Å. As expected, the more efficient packing of adjacent columns leads to a lower compressibility of the crystal in the directions of *a*- and *b*-axes. However, the large deviation of Cs atoms from the crown ether cavity results in a significant compression of the axis *c*. The unit-cell volume exhibits a monotonic decrease between the lowest and highest measured pressures, with an overall reduction of 280.1(4) $Å^3$ or 15.37% of the unit-cell volume. This volume compression exceeds that observed in the Rb complex (13.52%) at a pressure of 1.89 GPa. The pressure-volume (P–V) data presented in Figure 5 were analyzed using the EosFit software.[35] A third-order Birch-Murnaghan equation of state (EoS)[36] provided the best fit for the data. This analysis yielded a calculated zero-pressure volume (V_0) of 1827(5) $Å^3$ and a pressure bulk modulus (K_0) of 4.6(5) GPa, indicating a softer material compared to the rubidium complex with bulk modulus of 9.1(5) GPa due to its higher compressibility.

Additionally, the pressure derivative K′ was determined to be 13.7(1.6). This low bulk modulus is characteristic of soft materials, such as organic or metal-organic compounds, where intermolecular interactions are dominated by dispersion forces and/or electrostatic interactions.[37] Since we are comparing two isostructural compounds containing the same crown ether and $SbCl_6^-$ anions, such a dramatic difference in the bulk moduli values can only be explained by the very high compressibility of the Cs^+ cation compared to the Rb^+.

The cell parameters under pressure (P-a) and (P-c) generally follow the (P–V) dependence, exhibiting exponential trends as shown in the graphs. However, these dependencies become approximately linear within the pressure range 0.2–1.0 and 0.9–1.7 GPa. Utilizing the graphic-analytical method, we readily identify inflection points in the corresponding graphs around 0.9–1.0 GPa. The following sections will discuss the reason behind these inflection points and the deviations from the linear trend observed at pressure below 0.2 GPa and above 1.7 GPa.

It is noteworthy that at a pressure of 2.05(3) GPa, the a- and c-cell parameters of the Cs complex are only slightly longer by 0.012 Å and 0.058 Å, respectively, compared to the Rb complex at 1.89 GPa. Consequently, the unit cell volume is only about 12 $Å^3$ larger. This observation highlights the efficient compression of the Cs complex and suggests the possibility of arranging Cs atoms inside the crown ether cavity at a slightly higher pressure than for the Rb complex. Notably, the structural features of the corresponding salts at HP (around 2 GPa) are quite similar, despite the significant difference in unit cell volume (56.7 Å3) at ambient conditions and the larger radii of cesium cations compared to rubidium cations.

The Effect of Pressure on Interatomic Distances

Selected bond distances, contacts, and torsion angles in the crystal [Cs(18-Crown-6)][$SbCl_6$] at various pressures are listed in Table 2. Within the pressure range up to 2.05 GPa the shorter

Table 2. Selected bond distances, Cs–Cs separation, and torsion OCCO angles in crystal [Cs(18-Crown-6)][SbCl6] at various pressures. (* The deviation of the Cs from the crown ether plane is half of these values.)

Pressure (GPa)*	d(Cs–O)(min, max) (Å)	d(Cs–Cl) (Å)	d(Cs–Cs)* (Å)	d(Sb–Cl) (Å)	O–C–C–O, (°)
0.0(100 K)	2.9265(13), 3.0714(13)	3.5179(7)	1.7157(8)	2.3767(5)	70.6(2)
0.0	2.943(2), 3.091(2)	3.5891(13)	1.8977(16)	2.3762(10)	70.4(4)
0.04	2.937(3), 3.083(3)	3.5889(17)	1.827(2)	2.3698(11)	71.2(5)
0.23	2.918(2), 3.056(2)	3.5729(14)	1.6446(19)	2.3729(10)	70.9(4)
0.35	2.914(2), 3.046(3)	3.5707(16)	1.534(2)	2.3710(11)	72.2(5)
0.56	2.9025(18), 3.023(2)	3.5756(14)	1.3778(18)	2.3716(9)	72.3(4)
0.67	2.9014(19), 3.014(2)	3.5769(15)	1.2966(19)	2.3723(9)	72.6(4)
0.90	2.8923(19), 2.994(2)	3.5894(13)	1.1163(18)	2.3719(9)	73.3(4)
1.04	2.892(2), 2.987(2)	3.5968(12)	1.0244(17)	2.3725(8)	73.7(4)
1.20	2.8862(16), 2.9747(17)	3.6030(11)	0.9257(17)	2.3705(7)	74.0(3)
1.33	2.8872(18), 2.9700(19)	3.6112(12)	0.8619(19)	2.3701(8)	74.3(4)
1.57	2.8855(18), 2.9568(19)	3.6253(19)	0.741(4)	2.3713(8)	73.9(4)
1.69	2.8856(17), 2.9525(19)	3.610(3)	0.692(6)	2.3716(8)	74.3(4)
2.05	2.880(6), 2.929(8)	3.66(3)	0.51(6)	2.376(3)	72.3(12)
2.05c	2.894(6)	3.881(3)	0	2.376(3)	72.2(12)

c The Cesium atom was refined at the center of inversion. * Data collection for diffraction experiments performed at 293 K.

Research Article
doi.org/10.1002/ejic.202400222

Cs–O bond distances exhibit a relatively modest decrease by 0.063 Å square 2.943(2) to 2.880(6) Å, while the longer Cs–O bond distances decrease notably by 0.162 Å from 3.091(2) to 2.929(8) Å, leading to an average decrease of 0.113 Å in Cs–O bond distances. In general, shorter and longer Cs–O bond lengths significantly exceed those found for the isostructural rubidium complex(0.027 and 0.078 Å respectively). The geometry and conformational features of the crown ether remain unaffected by pressure, as demonstrated by the unaltered C–O and C–C bond distances and bond angles. Thus, it was found that the CO and CC bond distances in the structures at different pressures were in the range of 1.417–1.440(11) and 1.487–1.507(14) Å respectively. Additionally, the largest difference in CCOC and OCCO torsion angle values between the structure at ambient conditions and pressure of 2.05 GPa is about 1 and 4°. The geometry of the octahedral $SbCl_6^-$ anion is not sensitive to pressure, so Sb–Cl bond distances remain within a very tight range of 2.3698(11)–2.3762(10) Å, resulting in a maximum difference in bond lengths by 0.006 Å only. Therefore, the Sb–Cl bond lengths have the same value within 3σ in the reported pressure range. Analysis of Cs–Cl bond lengths shows that under pressure up to 1.69(3) GPa these bonds are in a fairly narrow range of values of 3.5797(16)-3.6263(19) Å. However, this trend is disrupted by a larger Cs–Cl distance (3.66(3) Å) observed at a pressure of 2.05(3) GPa. Two possible explanations exist for this outlier: 1) reduced data quality since at the HP crystal splitting and it might have compromised the X-ray diffraction data, leading to a decrease in reflection amplitudes during twinning data processing (this could have resulted in an inaccurate Cs–Cl bond length determination); 2) partial Cs-crown ether encapsulation at 2.05(3) GPa pressure, so the Cs atoms approach the entry barrier of the crown ether cavity (within 0.25–0.26 Å of the center). So, a part of Cs atoms may become partially encapsulated within the cavity and this mixed population (ordered and disordered Cs positions) could lead to an average Cs position closer to the center, resulting in slightly longer Cs–Cl distances and increased atomic displacement parameters (ADP) for Cs atoms. Similar Sb–Cl and Cs–Cl bond lengths in the range 2.344–2.385 Å and 3.618–3.745 Å respectively have been reported for the inorganic salt $CsSbCl_6$.[38] However, the Cs–Cl bond lengths found in the few compounds that have been found in CSD[15] and include $[Cs(18\text{-crown-6})]^+$ cation coordinated to different chlorine-containing anions such as Cl^-,[39] $SbCl_5^{2-}$,[11] and ECl_6^{2-} (where E=Te, Zr, Sn)[9] shows that these bonds are a bit shorter and in the range of 3.47–3.54 Å. In the last case with structural fragment $[Cs(18\text{-crown-6})][ECl_6]^{2-}$ the shortest H···Cl contacts between hydrogen atoms of the crown ether and anion are in the same range 3.26–3.33 Å as found for $[Cs(18\text{-Crown-6})][SbCl_6]$. Therefore, a significant lengthening of the Cs–Cl bonds at almost identical H···Cl contacts in the crystal can be explained by a noticeably smaller deviation of the cesium atom from the center of the crown ether in $[Cs(18\text{-Crown-6})][SbCl_6]$. These long distances indicate a relatively weak interaction between Cesium cations and the chlorine atoms in the crystal.

The Effect of Pressure on the Deviation of the Cs^+ Cation from the Crown Ether Cavity

Given the ionic radii of 1.81 Å for the Cl^- anion and 1.78 Å for the Cs^+ cation with a coordination number of 9,[40] one would expect a Cs–Cl bond distance around 3.59 Å. Notably, in $[Cs(18\text{-Crown-6})][SbCl_6]$, the Cs–Cl bond length aligns precisely with this expectation (3.5891(13) Å), although in the rubidium complex with smaller Rb^+ cation, the corresponding distance was significantly longer 3.7255(13) Å. This observation suggests that increasing pressure leads to a direct transfer of static pressure from the $SbCl_6^-$ anions to the Cs^+ cations, causing them to move immediately closer to the center of the crown ether cavity. This progressive shift of Cs^+ cations towards the crown centers with increasing pressure ultimately results in the gradual merging of two symmetry-related disordering components. As depicted in Figure 6, the pressure dependence of the Cs–Cs separation (P-d(Cs–Cs)) within this disordering scheme largely mirrors the behavior of the unit cell parameters in low pressure region. Within the pressure range up to approximately 1 GPa, the (P-d(Cs–Cs)) graph exhibits an exponential dependence, indicating a rapid convergence of the disordered Cs atoms towards the center of the crown ether cavity. This suggests an efficient transfer of static pressure from the anions to the cations at lower pressures. Beyond 1 GPa, the relationship transitions to a linear trend, implying a gradual slowing down of the convergence process. This could be due to steric hindrance in the molecule, such as shortening some intermolecular contacts in the crystal. The best fit for the (P-d) dependence across the entire pressure range was achieved using a third-order polynomial function in the form $P=A+Bd+Cd^2+Dd^3$, where A, B, C, and D are the fitted coefficients (1.8775, −1.0652, 0.2914, and −0.047, respectively). This model predicts that the Cs atoms would perfectly occupy the center of the crown ether cavity at a pressure of 3 GPa. Notably, a linear fit within the 1–2 GPa range yields the same predicted pressure.

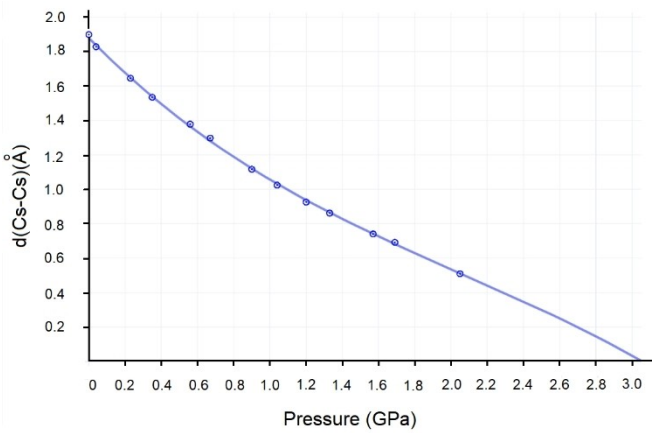

Figure 6. The dependence of the separation between two disordered positions of the Cs atom on pressure in $[Cs(18\text{-crown-6})][SbCl_6]$ crystal. The best fit approximation is made using the third order function $P=A+Bd+Cd^2+Dd^3$ in pressure range 0–2.05 GPa with the following A, B, C, and D coefficients: 1.8775, −1.0652, 0.2914, and −0.047, respectively, and P = pressure and d = d(Cs–Cs) separation.

Research Article
doi.org/10.1002/ejic.202400222

This pressure is only slightly higher than the value of 2.5 GPa required for the entry of a smaller rubidium cation into the center of the crown ether cavity in the isostructural compound. However, the slight downturn observed at high pressures (> 2 GPa) when considering the third-order function was also observed in the rubidium complex. The crown ether molecule adopts non-planar conformation, three oxygen atoms of crown ether reside slightly above and the other slightly below an average plane defined by all six O atoms. This results in an interplanar distance of about 0.5 Å. Under pressure 0–1.2 GPa, this distance increases from 0.47 Å to 0.56 Å. Interestingly, this increase coincides with a rise in the OCCO torsion angles, from 70.4(4)° to 74.3(4)°. Notably, the interplanar distance remains constant above 1.2 GPa. As mentioned before, when pressure increases, the shortest Cs–O distances steadily decrease to 2.880(6) Å at 2.05(3) GPa (see Table 2). This pressure corresponds to minimal Cs–O distance, where the disordered Cs atoms are shifted away from the center of the cavity by 0.255 Å (d(Cs–Cs) = 0.51(6) Å) since three oxygen and the cesium atoms occupy the position in the same plane. For a large ion like Cs, this suggests that the steric barrier to entering the cavity of the crown ether is located at a distance of approximately 0.22–0.25 Å from the center. When a Cs^+ cation, driven by external pressure, enters the cavity of the crown ether between the three closest oxygen atoms, it occurs in the center of the cavity surrounded by six oxygen atoms at equivalent distances but slightly longer Cs–O distances (2.894(6) Å) compared to the disordered model. This is due to the location of the cesium ion outside the planes of the oxygen atoms. While this value falls within the 3σ error range for Cs–O bonds of the disordered model, a clear trend emerges. However, partial penetration through the barrier by some Cs atoms introduces additional statistical disorder, with some residing in the center and others remaining outside. This explains the observed elongation of the ellipsoid of thermal vibrations for cesium atoms in the HP range and some descent observed in the graph in Figure 6 at pressures above 2.0 GPa.

It is worth noting that as soon as the pressure reaches 2.05(3) GPa, refinement of the structure becomes almost equally successful for the disordered model with Cs–Cs separation of 0.51(6) Å and ordered model when Cs occupied the position in the inversion center(Tables 1, 2 data labeled 2.05 and 2.05c). However, this ordered model yields slightly longer Cs–Cl bond distances (3.881(3) Å) and exceedingly large ADP values along z-axes for the Cs atoms due to the overlapping of the electron density for several disordered positions. A similar situation was observed for previously reported crystal Rb(18-crown-6)$SbCl_6$. It can be assumed, however, that at least some of the Cs^+ cations in the crystal at pressure around 2 GPa reside in the inversion centers.

The Effect of Pressure on Cl···H and H···H Contacts in Crystal

At ambient conditions, cations, anions, and crown ether are well-separated, as described previously. Consequently, no H···Cl or H···H contacts in the crystal approach the sum of their vdW radii (2.95 Å and 2.40 Å, respectively). The shortest C2–H2B···Cl1 contact between hydrogen and chlorine within columns is 3.24 Å. A bit shorter C1–H1B···Cl1^{i} contact between adjacent columns measures 3.10 Å, and the closest H···H contact is 2.74 Å, significantly exceeding the combined vdW radii of two hydrogen atoms. At pressure 0.9 GPa observed H···Cl contact of 2.95 Å which is equivalent to the sum of their vdW radii. As pressure increases to 2.05(3) GPa, the unit cell shrinks considerably, bringing cations and anions closer together. This compression significantly shortens the CH···Cl contacts within the crystal, reducing them to 2.81 Å. The list of H···Cl or H···H contacts as a function of pressure is shown in table 3. To investigate the dependence of short contacts H···Cl and H···H on pressure, we plotted the data from Table 3 on the graph shown in Figure 7. The points representing H···Cl contacts in columns along the c-axis and between adjacent columns in the ab plane are indicated in open blue circles and open red squares, respectively. The points representing H···H contacts between adjacent crown ethers are at the bottom and marked in open green triangles. The plots were smoothed using an exponential function. Corresponding distances at 2.95 Å and 2.40 Å represent the vdW interaction for H···Cl and H···H contacts, respectively. Interestingly, the intra-columnar H···Cl distance reaches the sum of their vdW radii (2.95 Å) around 0.95 GPa, as evident in the graph. Due to more efficient and substantial compression along the c-axis, the reduction in H···Cl contacts in this direction is notably larger. Similarly, inter-columnar H···Cl contacts reach 2.95 Å close to 0.9 GPa, indicating the convergence in both directions at similar pressures. Although initially longer by 0.14 Å, the intra-columnar H···Cl contact shortens rapidly, decreasing by 0.43 Å at 2.05(3) GPa compared to only 0.24 Å for inter-columnar contacts. Therefore, the graphs intersect at approximately 1.05 GPa. The H···H contacts between

Table 3. Shortest H···Cl and H···H contacts in crystal [Cs(18-Crown-6)][SbCl6] at various pressures.

Pressure (GPa)	H2b···Cl1 (Å)	H1b···Cl1^{i} (Å)	H2a···Cl1^{ii} (Å)	H1b···H1a^{ii} (Å)
0.0	3.24	3.42	3.10	2.75
0.04	3.20	3.39	3.07	2.72
0.23	3.14	3.29	3.05	2.65
0.35	3.10	3.23	3.02	2.63
0.56	3.04	3.17	3.00	2.58
0.67	3.02	3.13	2.96	2.57
0.90	2.96	3.07	2.95	2.53
1.04	2.93	3.04	2.94	2.51
1.20	2.90	3.01	2.91	2.47
1.33	2.89	2.99	2.91	2.47
1.57	2.86	2.96	2.89	2.43
1.69	2.85	2.95	2.88	2.43
2.05	2.81	2.93	2.86	2,35

The symmetry code: i = 1/3 + x–y, −1/3 + x, 2/3-z; ii = 1/3−y, −1/3 + x–y, −1/3 + z.

Research Article
doi.org/10.1002/ejic.202400222

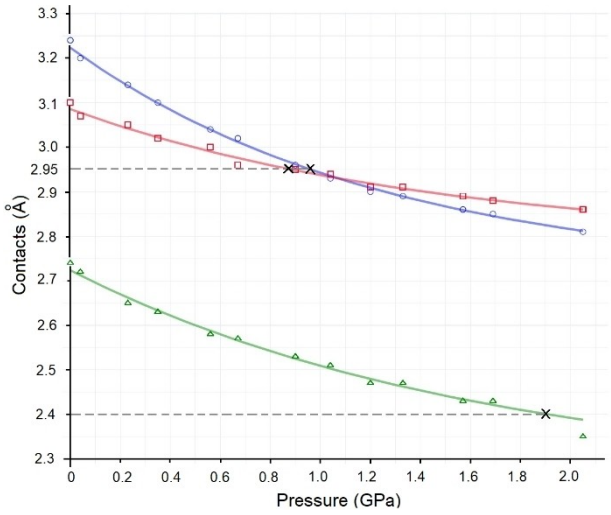

Figure 7. Length of H···Cl and H···H contacts as a function of pressure in [Cs(18-crown-6)][$SbCl_6$]. H···Cl contacts in columns and between adjacent columns in the *ab* plane are indicated with open blue circles and red open squares, respectively, and H···H contacts are marked as open green triangles. The black crosses indicate the pressure corresponding to the vdW contacts for the H/Cl and H/H atom pairs. The plots were smoothed using an exponential function.

adjacent crown ethers decrease by 0.39 Å under the applied pressure range but only approach the vdW radii (2.40 Å) at pressures exceeding 1.8–1.9 GPa. This suggests that H···H contacts do not significantly influence the relationships between pressure, unit cell parameters and volume at least up to 1.8–2.0 GPa. These data directly indicate that the detected inflection points in the graphs of the cell parameters versus pressure (P-a) and (P-c) are associated with the appearance of shortened H···Cl contacts in the crystal.

Voids Analysis

Typically, in non-porous molecular crystals, at least 20% of the unit cell volume remains unoccupied at ambient pressure.[41] The [Cs(18-Crown-6)][$SbCl_6$] crystal possesses numerous voids between molecules at ambient pressure, evident from the lack of close H···Cl and H···H interactions. So, all intermolecular interactions exceed the sum of their vdW radii at atmospheric pressure. To estimate the volume occupied by molecules and voids, the crystallographic data at various pressures were analyzed using the contact surface mapping method in Mercury software (version 2023.3.0).[42] The probing radius and step were set to 0.2 Å. Complete data with the detailed void volume data in the [Cs(18-Crown-6)][$SbCl_6$] crystal at different pressures is presented in Table 4. Since the cesium complex at ambient conditions exhibits elongation of the unit cell along the *c*-axis compared to rubidium one, this results in a larger total unit cell volume and void volume (57 $Å^3$ and 22 $Å^3$, respectively). The void volume at ambient pressure is 490.9 $Å^3$, representing 26.9% of the unit cell volume. While the total void volume in the crystal is significant, its distribution across small interstitial spaces around and between molecules prevents the accommodation of even small guest molecules like water. This compares to 468.5 $Å^3$ and 26.5% observed in the isostructural [Rb(18-crown-6)][$SbCl_6$] complex. As pressure increases to 2.05(3) GPa, the void volume in the [Cs(18-Crown-6)][$SbCl_6$] crystal shrinks to 224.7 $Å^3$, representing 14.6% of the unit cell. This value closely resembles the void volume (226.3 $Å^3$) observed in the Rb complex at a slightly lower pressure (1.89 GPa). Based on the observed coincidence of the inflection point on the graph (P-Void), as well as with the inflection points on the graphs (P-a), (P-c) and the shortening of the H···Cl contacts to 2.95 Å at a pressure about 0.9 GPa, we can conclude that a compelling connection emerges. It suggests that observed inflection points might be directly linked to the appearance of short H···Cl contacts Figure 8 presents the complete data of void volume dependence on pressure (P-Voids). The data closely follows an exponential trend (red line), but two distinct and linear regions (marked as blue lines) with an intersection at a point near 0.95 GPa are visible: one between 0.2–0.9 GPa and another between 1–1.7 GPa (blue lines). This interpretation aligns with

Table 4. Total void volume ($Å^3$) in the crystal [Cs(18-Crown-6)][SbCl6] at various pressures.

Pressure (GPa)[1]	Total void Volume ($Å^3$)	% of unit cell volume
0.0	490.9	26.9
0.04	476.1	26.3
0.23	417.5	23.7
0.35	393.5	22.7
0.56	359.2	21.2
0.67	341.8	20.4
0.90	307.2	18.7
1.04	290.5	17.8
1.20	273.6	17.0
1.33	263.7	16.5
1.57	248.0	15.7
1.69	239.1	15.2
2.05	224.7	14.6

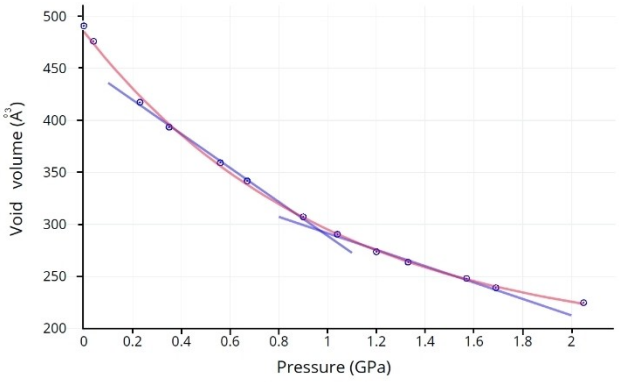

Figure 8. Total void volume in the [Cs(18-crown-6)][$SbCl_6$] at various pressures. (The voids were calculated using the contact surface maps method, the probing radius and the step was set up to 0.2 Å.)

Research Article
doi.org/10.1002/ejic.202400222

the observation that void compression becomes more difficult at a pressure around 0.95 GPa, with the slowing down of the cesium atom's approach towards the center of the crown ether cavity, indicating a decreased availability of "easy" compression pathways within the voids. The plot's initial, rapid decrease in void volume up to 0.2 GPa likely reflects two contributing factors: slight compression of the bulky cesium cations as they approach the crown ether cavity and attractive forces acting at distances close to the vdW radii of the atoms contribute to this volume reduction before any significant short-range interactions form. Finally, at pressures above 1.7 GPa, a further decrease in compressibility is observed, which can be attributed to the emergence of shortened H···H contacts within the crystal. These data allow us to conclude that the main factor determining the efficiency of compression of crystals under pressure is not just the physical presence of voids, but the presence/absence and subsequent shortening of intermolecular contacts in the crystal. As these contacts shorten and approach the sum of their vdW radii under increasing pressure, they act as points of additional internal crystal resistance, effectively modulating the compressibility. This knowledge could be invaluable in tailoring materials for specific applications requiring controlled compressibility of the material.

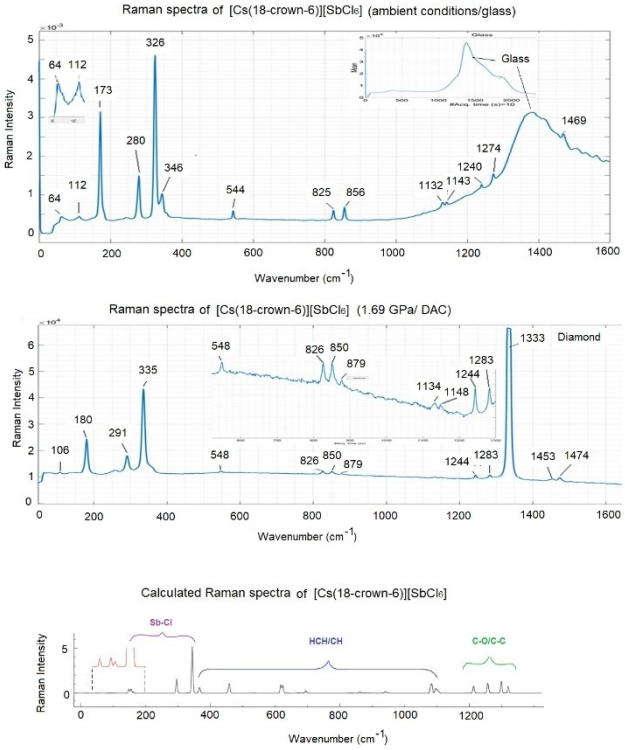

Figure 9. Raman spectra of the [Cs(18-crown-6)][$SbCl_6$]: (top) recorded from crystal at ambient conditions placed on top of the glass plate; (middle) recorded from the crystal inside diamond anvil cell under pressure 1.69 GPa (at 1333 cm^{-1} strong Raman signal from the diamond is observed); (bottom) Raman spectra calculated by DFT methods at ambient conditions.

Raman spectra and Quantum Chemical Calculations

The impact of pressure on the spectral properties of [Cs(18-Crown-6)][$SbCl_6$] was investigated using Raman spectroscopy. To perform Raman spectroscopy single crystal was placed on a glass plate and studied at ambient pressure and within a diamond anvil cell (DAC) at 1.69 GPa. The obtained spectra are presented in Figure 9. The most prominent Raman shift vibration modes reside in the low-frequency region of 170–340 cm^{-1} and are attributed to Sb–Cl vibrations. Relatively weak signals at 350–1500 cm^{-1} correspond to various vibrations within the crown ether, involving C–H, C–C, and C–O bonds. At ambient conditions, well-defined but weak vibration modes were observed at very low frequencies, specifically at 64 and 112 cm^{-1}. Under increasing pressure, most Raman signals exhibit a blue shift of up to 9 cm^{-1}. Notably, the weak signal at 112 cm^{-1} undergoes a redshift of 6 cm^{-1} instead, and the signal at 64 cm^{-1} is degraded. Density functional theory (DFT) calculations were performed to evaluate the molecules' energy characteristics. The geometry of the model molecules in calculations was not optimized, for single-point calculations the atomic coordinates after generation symmetry equivalent positions for all atoms were taken from the X-ray diffraction experiments. Energies of model molecules were estimated at ambient conditions, 1.69 and 2.05 GPa. The difference in energy between the most favorable molecule at ambient conditions and the corresponding pressure of 1.69 and 2.05 GPa for disordered and ordered cesium atoms, was 4.8, 5.4, and 7.7 kcal/mol, respectively. These results demonstrate that the energetic difference between disordered and ordered (with Cs atoms inside crown ether cavity) models at 2.05 GPa was only about 2 kcal/mol. Therefore, expecting a completely ordered model with Cs atoms inside the crown ether cavity at pressures around 3 GPa is reasonable. We employed quantum chemistry calculation methods for vibrational frequency analysis to identify all peaks in the Raman spectra. We calculated IR and Raman spectra of the molecule at ambient pressure and under pressure of 1.69 GPa to compare with experimental Raman spectra. These calculations were performed for isolated molecules in a vacuum, neglecting the influence of crystal field forces. The calculated positions of Sb–Cl Raman vibrational modes agreed well with the experimental data, for example, at normal pressure the strongest signal at 333 cm^{-1} is assigned to totally symmetric breathing mode of $SbCl_6^-$ anion, the vibration of doubly degenerate in O_h symmetry is split into two components at 289 cm^{-1} and third vibration at 154–161 cm^{-1}, normally seen in the Raman spectrum of octahedral species, is the triply degenerate in-plane bend.[43] It is easy to see that the presented Raman vibration modes practically coincide with those detected in the experiment.

However, the vibrational modes of CH, CC, and CO bonds (340–1470 cm^{-1}) were compressed into a narrower frequency range and shifted towards lower frequencies in the calculations. Due to the low symmetry of the calculated model crown ether molecule, the number of vibrational modes in the calculated spectrum was large, so we will not discuss this here, but the calculated spectra look quite close to the real ones. The ORCA output file revealed also low-intensity Raman signals at 67 cm^{-1} and 114 cm^{-1} under ambient conditions as in experimental

Research Article
doi.org/10.1002/ejic.202400222

Raman spectra. These signals correspond to Cs atom vibrations: the first in the direction perpendicular to the crown ether plane (towards the anion), and the second, split signal, in the plane of the crown ether oxygen atoms, respectively. Additionally, in this region, a very weak signal at 101 cm^{-1} was assigned to Sb–Cl vibrations. According to calculations, at a pressure of 1.69 GPa, the low-frequency signal (67 cm^{-1}) corresponding to Cs vibration exhibited a decrease in intensity and a red shift of 11 cm^{-1}. This vibrational mode is associated with the entire $[Cs(18\text{-crown-6})]^+$ species, not the Cs^+ cation alone as at ambient conditions. Conversely, the in-plane Cs vibration (114 cm^{-1}) underwent a blue shift of 27 cm^{-1}. Notably, the weak Sb–Cl vibration signal at 101 cm^{-1} remained almost unchanged in both intensity and frequency. Interestingly, the intensities of CH, CO, and CC vibrations displayed a redshift of 6–10 cm^{-1}, which can be attributed to the absence of intermolecular interactions when simulating the spectral properties of the molecule in a vacuum.

Conclusions

There are no shortened intermolecular contacts in the crystal at relatively low pressures. The low value of pressure bulk modulus (5.5 GPa) makes this hybrid organic-inorganic crystal comparable to various organic and organometallic compounds, for which dispersive and/or electrostatic interaction forces predominate. The high compression rate of [Cs(18-Crown-6)][$SbCl_6$] crystals at relatively low pressure can be attributed to the absence of shortened H···Cl and H···H intermolecular contacts in the crystal and the "soft" nature of the large Cs^+ cations. The nonlinear dependence of unit cell parameters on pressure with the inflection point at around 0.95 GPa can be explained by the influence of shortened intermolecular contacts in the crystal. At pressures exceeding 0.9–1 GPa, steric repulsion forces become increasingly influential due to the shortening of several interatomic H···Cl and H···H contacts in the crystal to distances below the sum of their vdW radii. Compression of crystal, accompanied by a significant void reduction, leads to the rapid approach of Cs atoms toward the center of the crown ether cavity. The void reduction under pressure also demonstrates two linear sections with the inflection point at 0.95 GPa. Collectively, these factors play an important role in the behavior of [Cs(18-Crown-6)][$SbCl_6$] crystal under pressure. To force the Cs atom inside the center of the crown ether cavity, pressures of about 3 GPa are required. The highly symmetric structure of [Cs(18-Crown-6)][$SbCl_6$] and a limited number of specific hydrogen-bonding interactions with neighboring molecules make it a particularly valuable model for studying the influence of interatomic interactions in crystals under high pressure. This simplified system allows us to isolate and investigate the effects of pressure on specific interatomic interactions without the additional complexity of numerous and diverse forces present in more complex systems. While alternative approaches may be needed for other systems, compound 1 presents a powerful tool for gaining fundamental insights into pressure-induced changes in interatomic interactions and their impact on various material properties.

Experimental Part

Preparing the Crystal and the DAC for the Experiment

The [Cs(18-Crown-6)][$SbCl_6$] were synthesized and recrystallized from the DMF using the procedure described earlier.[21] Before the HP experiments, the best quality crystal with a size 0.11×0.12×0.14 mm was selected for the diffraction experiments. The compression of a single crystal in experiments was carried out using a Diacell ® Tozer diamond anvil cell (DAC) equipped with Boehler–Almax cut diamonds with 0.8 mm culets. For the experiments, the gaskets, made of 0.25 mm BeCu alloy foil, were preintended to a thickness of 0.2 mm. A spark-eroded hole with a diameter of 0.35 mm was created using Loto Eng. Spark E400. In a series HP diffraction experiments [at pressures of 0.04(3). 0.23(3) 0.35(3), 0.56(3), 0.67(3), 0.90(3), 1.04(3), 1.20(3), 1.33(3), 1.57(3), 1.69(3) and 2.05(3)GPa)], a mixture of pentane-isopentane (1 : 1) was used as a pressure-transmitting medium. This hydrostatic medium is very volatile (bp ~35 °C), therefore, the DAC and hydrostatic medium were cooled to −17 °C in a fridge before loading. The crystal and ruby ball were glued to the DAC culet using a minimal amount of transparent epoxy resin without hardener. The cell was loaded with the selected crystal, reference ruby ball for the pressure control, and pressure transmitting medium, and then immediately sealed. After visual inspection for the absence of air bubbles inside, the DAC was placed into a T-press (LOTO-eng.) for compression and the step-by-step load to the TozerDAC was applied. The pressure inside the DAC was monitored before and after each diffraction experiment by the ruby fluorescence pressure measurement method[44] with an accuracy of ±0.03 GPa. The pressure control with the following data collection on the diffractometer was performed with a delay of 10 min after the pressure rise. To obtain high-quality diffraction data from large crystals with high I/σ(I) ratio, we employed a metal gasket of considerable thickness and a large-diameter hole. This resulted in an expansion of the working chamber volume and an outward displacement of the gasket at a pressure of around 2 GPa. Since the crystal was crushed between the anvils in an attempt to raise the pressure, further data collection including pressure release was not performed. To perform the HP experiment, a single-cup beamstop with a larger crystal-to-beamstop distance was installed to create enough space for the HP cell. The crystal-to-detector distance was set up to 60 mm. Then a Victrex PEEK 450 g holder together with the HP Tozer DAC was fixed into the goniometer head and the crystal was readily centered on the diffractometer.[45,46]

Data Collection/Reduction/Refinement Details

The diffraction data were collected at 293 K on a Rigaku XtaLAB Synergy-S diffractometer equipped with the PhotonJet-S microfocus Mo X-ray source with a mirror design and hybrid photon counting HyPix-6000HE detector. An exposure time of 3–5 seconds per 1 degree was estimated as the target for the data collected. The processing procedures for the HP experiments to a resolution of 0.75 Å were followed by procedures implemented in CrysAlisPro software.[47] The integrations were carried out using dynamic masking of the regions of the detector shaded by the HP cell. The final data reduction was performed to opening angles of 38°. The crystal structure was solved by direct methods and refined by the full-matrix least-squares on F^2 for all reflections using SHELXL[48] operated under OLEX2,[49] these coordinates were then used for

refinement at subsequent pressure points. The non-hydrogen atoms were refined freely with anisotropic displacement parameters. All H atoms were placed at calculated positions and refined as riding, with C–H = 0.97 Å and Uiso(H) = 1.2Ueq(C). At a maximal pressure of 2.05 GPa crystal inside DAC was cracked between diamond anvils for several fragments and thus diffraction quality was not so good. In addition, the structure refinement at 2.05 GPa becomes almost equally successful for Cs sitting on the inversion center or for the disordered model with d(Cs··Cs) = 0.51(6) Å. However, this ordered model yields longer Cs–Cl bond distances of 3.881(3) Å compared to values of 3.60 ± 0.03 Å found at pressure range 0–1.69 GPa and exceedingly large ADP values along z-axes for the Cs atoms. Deposition Numbers 2348747–2348760 contain(s) the supplementary crystallographic data for this paper. These data are provided free of charge by the joint Cambridge Crystallographic Data Centre and Fachinformationszentrum Karlsruhe Access Structures service.

Raman Spectroscopy and Quantum Chemical Calculations

The Raman spectra were recorded with a Horiba LabRAM HR Evolution UV-VIS-NIR. To perform Raman spectroscopy with 785 nm laser excitation a single crystal was placed on a glass plate and studied at ambient pressure and within a diamond anvil cell (DAC) at 1.69 GPa. Gas phase density functional theory (DFT) calculations were performed employing the BP86[50,51] functionals implemented in the ORCA 5.0.2 software package.[52] For calculations involving Sb/Cs atoms, the segmented all-electron relativistically contracted basis set (SARC-ZORA-TZVP)[53] was employed. For calculations involving C, H, O, and Cl atoms, the ZORA-def2-TZVP basis set[54] was used in combination with the corresponding SARC/J auxiliary basis set.[55] Relativistic effects were accounted for using the zero-order regular relativistic approximation (ZORA).[56–57]

Acknowledgements

ER acknowledges funding from the Swiss National Science Foundation and Scholar at Risk for grant support (Grant IZSEZ0_212011/IZSEZ0_216018). This work was supported by the Ministry of Education and Science of Ukraine (Project no. 22BF037-11). Dr. Simon Bohme acknowledged for Raman spectroscopy. Open Access funding provided by Eidgenössische Technische Hochschule Zürich.

Conflict of Interests

The authors declare no conflict of interest.

Data Availability Statement

Data sharing is not applicable to this article as no new data were created or analyzed in this study.

Keywords: Single crystal X-Ray diffraction · high pressure · 18-Crown-6 · Raman spectra · DFT calculations

[1] J. W. Steed, *Coord. Chem. Rev.* **2001**, *215*, 171–221.
[2] S. Di Stefano, G. Capocasa, L. Mandolini, *Eur. J. Org. Chem.* **2020**, 3340–3350.
[3] D. A. Wynn, M. M. Roth, B. D. Pollard, *Talanta.* **1984**, *31*, 1036–1040.
[4] a) G. V. Gokel, W. M. Leevy, M. E. Weber, *Chem. Rev.* **2004**, *104*, 2723–2750; b) J. W. Steed, *Coord. Chem. Rev.* **2001**, *215*, 171–221.
[5] G. Chehardoli, A. Bahmani, *Supramol. Chem.* **2019**, *31*, 221–238.
[6] X. Y. Song, T. Zhang, Z. X. Gu, Z. X. Zhang, D. .-W. Fu, X. .-G. Chen, H. U. Zhang, R.-G. Xiong, *J. Am. Chem. Soc.* **2021**, *143*, 5091–5098.
[7] a) R. Chen, Y. Hui, B. Wu, Y. Wang, X. Huang, Z. Xu, P. Ruan, W. Zhang, F. Cheng, W. Zhang, J. Yin, J. Li, N. Zheng, *J. Mater. Chem. A.* **2020**, *8*, 9597–9606; b) J. W. Steed, *Coord. Chem. Rev.* **2001**, *215*, 171–221.
[8] Y. .-X. Xie, G. .-J. Yuan, J. .-B. Miao, Y. .-T. Luan, L. Li, H. Chen, X. .-M. Ren, *Dalton Trans.* **2022**, *51*, 15158–15165.
[9] C. Zhu, J. Jin, M. Gao, A. M. Oddo, M. C. Folgueras, Y. Zhang, C. .-K. Lin, P. Yang, *J. Am. Chem. Soc.* **2022**, *144*, 12450–12458.
[10] P. Ferdowsi, U. Steiner, J. V. Milić, *J. Phys. Mater.* **2021**, *4*, 042011.
[11] V. Morad, S. Yakunin, M. V. Kovalenko, *ACS Materials Lett.* **2020**, *2*, 845–852.
[12] J. A. Rusanova, K. V. Domasevitch, O. Yu Vassilyeva, V. N. Kokozay, E. B. Rusanov, S. G. Nedelko, O. V. Chukova, B. Ahrens, P. R. Raithby, *J. Chem. Soc. Dalton Trans.* **2000**, 2175–2182.
[13] K. V. Domasevitch, V. V. Ponomareva, E. B. Rusanov, T. Gelbrich, J. Sieler, V. V. Skopenko, *Inorg. Chim. Acta.* **1998**, *268*, 93–101.
[14] J. A. Manskaya, K. V. Domasevitch, V. V. Ponomareva, J. Sieler, V. N. Kokozay, *Z. Naturforsch.* **1998**, *53b*, 683–688.
[15] C. R. Groom, I. J. Bruno, M. P. Lightfoot, S. C. Ward, *Acta Crystallogr. Sect. B* **2016**, *72*, 171–179.
[16] J. J. Kiernicki, M. Zeller, N. K. Szymczak, *Inorg. Chem.* **2020**, *59*, 9279–9286.
[17] K. V. Domasevitch, J. A. Rusanova, O. Y. Vassilyeva, V. N. Kokozay, P. J. Squattrito, J. Sieler, P. R. Raithby, *J. Chem. Soc. Dalton Trans.* **1999**, 3087–3093.
[18] Z. Zhou, R. K. Kawade, Z. Wei, F. Kuriakose, O. Ungör, M. Jo, M. Shatruk, R. Gershoni-Poranne, M. A. Petrukhina, I. V. Alabugin, *Angew. Chem. Int. Ed.* **2020**, *59*, 1256–1262.
[19] K. V. Domasevitch, V. V. Ponomareva, E. B. Rusanov, *J. Chem. Soc. Dalton Trans.* **1997**, 1177–1180.
[20] S. N. Spisak, Z. Zhou, S. Liu, Q. Xu, Z. Wei, K. Kato, Y. Segawa, K. Itami, A. Y. Rogachev, M. A. Petrukhina, *Angew. Chem. Int. Ed.* **2021**, *60*, 25445–25453.
[21] V. V. Ponomarova, J. A. Rusanova, E. B. Rusanov, K. V. Domasevitch, *Acta Crystallogr.Sect. C* **2015**, *71*, 867–872.
[22] J. A. R. P. Sarma, R. Diseraju, *Acc. Chem. Res.* **1986**, *19*, 222–228.
[23] M. Podsiadło, A. Olejniczak, A. Katrusiak, *CrystEngComm.* **2014**, *16*, 8279–8285.
[24] G. M. Espallargas, L. Brammer, D. R. Allan, C. R. Pulham, N. Robertson, J. E. Warren, *J. Am. Chem. Soc.* **2008**, *130*, 9058–9071.
[25] M. Bujak, M. Podsiadło, A. Katrusiak, *CrystEngComm.* **2016**, *18*, 5393–5397.
[26] Z. Fu, Z. Yang, X. Yang, K. Wang, B. Zou, *Chem. Sci.* **2023**, *14*, 4817–4823.
[27] A. Katrusiak, *Acta Crystallogr. Sect. B* **2019**, *75*, 918–926.
[28] I. Orgzall, F. Emmerling, B. Schulz, O. Franco, *J. Phys. Condens. Matter.* **2008**, *20*, 295206.
[29] N. Giordano, S. Afanasjevs, C. M. Beavers, C. L. Hobday, K. V. Kamenev, E. F. O'Bannon, J. Ruiz-Fuertes, S. J. Teat, R. Valiente, S. Parsons, *Molecules.* **2019**, *24*, 2018.
[30] M. Kaźmierczak, A. Katrusiak, *J. Phys. Chem. C.* **2013**, *117*, 1441–1446.
[31] A. Bondi, *J. Phys. Chem.* **1964**, *68*, 441–451.
[32] E. B. Rusanov, M. D. Wörle, M. V. Kovalenko, K. V. Domasevitch, J. A. Rusanova, *Acta Crystallogr. Sect. B* **2024**, *80*, 135–145.
[33] S. Mattia, F. Fischer, K. Frederik, K. Hidetaka, B. J. Bo, *Angew. Chem. Int. Ed.* **2017**, *56*, 3625–3629.
[34] M. Blackman, I. H. Khan, *Proc. Phys. Soc.* **1961**, *77*, 471–475.
[35] J. Gonzalez-Platas, M. Alvaro, F. Nestola, R. Angel, *J. Appl. Crystallogr.* **2016**, *49*, 1377–1382.
[36] R. J. Angel, *Rev. Mineral. Geochem.* **2000**, *39*, 85–104.
[37] R. J. Angel, High-Pressure Crystallography, NATO Science Series II; A. Katrusiak, P. McMillan, Eds.; Kluwer Academic Publishers: Dordrecht; Boston, **2004**, *140*, 21–36.
[38] E. G. Zaitseva, S. V. Medvedev, L. A. Aslanov, *J. Struct. Chem.* **1990**, *31*, 92–97.
[39] N. van Well, C. Klein, F. Ritter, W. Assmus, C. Krellnera, M. Bolte, *Acta Crystallogr. Sect. C* **2014**, *70*, 455–459.
[40] R. D. Shannon, *Acta Crystallogr. Sect. A* **1976**, *32*, 751–767.

Research Article
doi.org/10.1002/ejic.202400222

[41] C. J. G. Wilson, T. Cervenka, P. A. Wood, S. Parsons, *Cryst. Growth Des.* **2022**, *22*, 2328–2341.
[42] C. F. Macrae, I. Sovago, S. J. Cottrell, P. T. A. Galek, P. McCabe, E. Pidcock, M. Platings, G. P. Shields, J. S. Stevens, M. Towler, P. A. Wood, *J. Appl. Crystallogr.* **2020**, *53*, 226–235.
[43] B. H. Christian, M. J. Collins, R. J. Gillespie, J. F. Sawyer, *Inorg. Chem.* **1986**, *25*, 777–788.
[44] G. J. Piermarini, S. Block, J. D. Barnett, R. A. Forman, *J. Appl. Phys.* **1975**, *46*, 2774–2780.
[45] P. Dera, A. Katrusiak, *J. Appl. Crystallogr.* **1999**, *32*, 510–515.
[46] H. E. King, L. W. Finger, *Appl. Crystallogr.* **1979**, *12*, 374–378.
[47] Agilent *CrysAlis PRO*. Agilent Technologies Ltd, Yarnton, Oxfordshire, England, **2014**.
[48] G. M. Sheldrick, *Acta Crystallogr. Sect. C* **2015**, *71*, 3–8.
[49] O. V. Dolomanov, L. J. Bourhis, R. J. Gildea, J. A. K. Howard, H. Puschmann, *J. Appl. Crystallogr.* **2009**, *42*, 339–341.
[50] A. D. Becke, *J. Chem. Phys.* **1986**, *84*, 4524–4529.
[51] J. P. Perdew, *Phys. Rev. B* **1986**, *33*, 8822–8824.
[52] F. Neese, *Wiley Interdiscip. Rev.: Comput. Mol. Sci.* **2018**, *8*, e1327.
[53] J. D. R. Rolfes, F. Neese, D. A. Pantazis, *J. Comput. Chem.* **2020**, *41*, 1842–1849.
[54] F. Weigend, R. Ahlrichs, *Phys. Chem. Chem. Phys.* **2005**, *7*, 3297–3305.
[55] F. Weigend, *Phys. Chem. Chem. Phys.* **2006**, *22*, 1057–1065.
[56] C. van Wüllen, *J. Chem. Phys.* **1998**, *109*, 392–399.
[57] E. van Lenthe, E. J. Baerends, J. G. Snijders, *J. Chem. Phys.* **1993**, *99*, 4597–4610.

Manuscript received: April 17, 2024
Revised manuscript received: May 17, 2024
Accepted manuscript online: May 22, 2024
Version of record online: June 27, 2024